Asian Journal of Chemistry; Vol. 31, No. 4 (2019), 917-924

ASIAN JOURNAL OF CHEMISTRY

https://doi.org/10.14233/ajchem.2019.21850

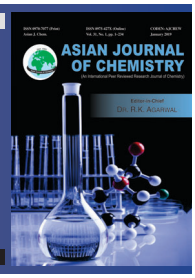

Photoluminescence and γ-Ray Induced Thermoluminescence Investigation of Phase Pure Cerium Doped Yttrium Silicate Nanophosphors

K. DHANALAKSHMI[1,2,*], A. JAGANNATHA REDDY[3] and L. PARASHURAM[4]

[1]Department of Physics, New Horizon College of Engineering, Bangalore-560103, India
[2]Research and Development Center, Bharathiar University, Coimbatore-641046, India
[3]Department of Physics, M.S. Ramaiah Institute of Technology, Bangalore-560054, India
[4]Department of Chemistry, New Horizon College of Engineering, Bangalore-560103, India

*Corresponding author: E-mail: dhanalakshmi.kurakula@gmail.com

Received: 27 November 2018; *Accepted*: 11 January 2019; *Published online*: 27 February 2019; AJC-19307

$Y_2SiO_5:Ce^{3+}$ (1-7 mol %) nanophosphors were prepared by solution combustion method using oxalyldihydrazide fuel. The phosphors were characterized by X-ray diffraction, scanning electron microscopy, UV-visible and Fourier transform infrared spectroscopy. The XRD patterns confirm the monoclinic structure of the prepared phosphors, with crystallite size of 66-74 nm. The surface morphology and elemental composition were evaluated by SEM and energy dispersive X-ray analysis. The optical band gap was calculated and is between 4.66 eV – 4.9 eV. The presence of Si-O-Si and Y-O bonds was confirmed by the FTIR spectra. Effect of cerium concentration on photoluminescence and thermoluminescence intensity were interpreted. The photoluminescence emission spectrum was recorded under excitation wavelength of 370 nm, the emission spectra showed three significant peaks positioned at 418 nm, 459 nm and 485 nm, which are ascribed to electronic transitions between 5d-4f levels. The nature and activity of trap centers were evaluated from the parameters obtained from Chen′s peak shape method. The intense blue emission by phosphor makes it a competent material for blue emission display devices. Also, its thermoluminescence properties make it a good material for dosimetric applications.

Keywords: Yttrium silicate, Cerium, Photoluminescence, Thermoluminescence, Nanophosphors.

INTRODUCTION

Recently research on rare-earth doped luminescent materials have attained greater importance for their potential applications in the fields of optics such as, phosphors [1], lasers [2], fiber amplifiers [3], optical storage [4], display devices [5]. Rare earth doped luminescent nanomaterials play a vital role in deciding their uniqueness in the specific applications. However, progress in the development of such materials has been scanty. In this path, zinc, calcium and strontium based phosphors are dominant and proven to be more efficient [6]. But the draw backs like degradation life time, stability and phase purity *etc*., have caused constraints for further technological advancements. Yttrium silicate (Y_2SiO_5) is an important luminescent host material for various rare earth activators. It is a refractory silicate with a high melting point, hence finds application as high-temperature luminescent phosphor [7].

Thermal stabilized solid yttrium silicate can be used in extreme conditions because of its linear thermal expansion and resistance to erosion [8]. Doping rare earth elements into Y_2SiO_5 gives materials with improved optical properties, making them competent candidates in the field of optical materials. Besides the excellent structural and optical characteristics of silicates, not much attention was focused by the scientific community on these yttrium silicate nanomaterials compared to sulphide nanomaterials and quantum dots, *etc*. Yttrium silicate finds superior applications over sulphide phosphors, due to its excellent optical clarity, high luminescence output, chemical stability [9-12] and chemical resistance [13]. High luminescence intensity and low decay time of cerium makes it a dopant to enhance the optical properties of host materials [14]. Saha *et al*. [15] investigated the effect of crystal structure and crystal size on the photoluminescence properties of Ce^{3+} doped yttrium silicate nanocrystals. Guerbous and Boukerika [16] reported the synthesis

of YAG:Ce nanophosphors by sol-gel method, these YAG:Ce nanophosphors showed intense green-yellow emission corresponding to Ce^{3+} $^5d_1 \rightarrow {}^2F_{5/2}, {}^2F_{7/2}$ transitions [16]. Several preparation methods have been used for the preparation of rare earth doped phosphors, which include co-precipitation method [17], sol-gel chemistry [18], hydrothermal synthesis [19], solvothermal [20], solid state reaction [21] and combustion synthesis [22]. Among these methods, the solution based combustion chemistry offers relatively low cost, facile and fast preparation process, formation of high-purity products and formation of virtually any size and shape products [23]. Hence the method has great control over the stoichiometric composition, repeatability and large scale preparation [24]. To our best of knowledge, there were no reports on thermoluminescenc properties of combustion processed cerium doped yttrium silicate under γ-irradiation. Hence, in this paper we report the synthesis of cerium doped yttrium silicate nanophosphor by facile solution combustion route. An investigation of thermoluminescent properties under γ-irradiation was carried out, the experimental parameters indicates that cerium doped yttrium silicate is a good competitor for dosimetric applications.

EXPERIMENTAL

Synthesis of cerium doped yttrium silicates phosphors

Synthesis of Y_2SiO_5: The cerium(III) nanophosphors were done by combustion method. The raw materials yttrium oxide (Y_2O_3), fumed silica (SiO_2) and cerium oxide (Ce_2O_3) were taken as the sources of yttrium, silicon and cerium. Depending on the total oxidizing and reducing valency of the compounds, the stoichiometry of the redox mixture was calculated for the combustion method. Stoichiometric amount of Ce_2O_3 (1-7 mol %) was taken in a petri-dish, to which 10 mL of 1:1 HNO_3 was added, the mixture was heated on a sand bath till excess nitric acid was removed. To this solution, appropriate amount of Y_2O_3, SiO_2, oxalyldihydrazide fuel and 20 mL of distilled water were added. This mixture was stirred well using magnetic stirrer to produce homogeneous mixture. Thus obtained mixture was kept in a preheated muffle furnace at 500 ºC, the mixture under went dehydration with the evolution of gases. The gel type product underwent auto-ignition and converted into powder. The resulting product was ground to fine powder and calcined at 1300 ºC for 3 h. Following the procedure different mole % cerium doped Y_2SiO_5 phosphors have been prepared.

Instrumentation: Powder X-ray diffractometer (Shimadzu 7000 s, CuKα (1.54 Å) equipped with a nickel filter was used to obtain the diffraction data. FTIR studies were performed on a Perkin Elmer spectrometer (Spectrum 1000) using KBr pellets. The morphology and structure of nanophosphors were examined by SEM (Hitachi). The absorption spectra of the samples were recorded on a SL-159 ELICO UV-Vis spectrophotometer. The photoluminescence (PL) measurements were performed on a Varian Cary Eclipse Photoluminescence spectrofluorimeter. Thermoluminescence measurements were carried out using Nucleonix TL reader with Co-60 γ-ray as irradiation source.

RESULTS AND DISCUSSION

Structural analysis: Crystallite size and strain in undoped and doped phosphors were estimated by X-ray diffraction patterns, shown in Fig. 1. The peaks positioned at 2θ values 22º, 25º, 28º, 30º, 34º, 44º, 48º, 49º, 50º and 58º were indexed to (2 1 1), (2 0 2), (-1 21), (2 2 0), (-321), (-602), (31 4), (-5 2 3), (-4 1 5) and (1 1 6), respectively. The patterns are in good agreement with the crystal structure data of Y_2SiO_5 with card number 36-1476. Lattice parameters evaluated from the data are a = 14.4021 Å, b = 6.7210 Å, c = 10.410 Å and α = 90º, β = 122.20º and γ = 90º, which indicate monoclinic structure of Y_2SiO_5. Absence of impurity peaks indicates the formation of phase pure crystalline phosphors. crystallite size (D) of pure and doped nanophosphors were calculated using Scherer′s method [25]:

$$D = \frac{K\lambda}{\beta\cos\theta} \quad (1)$$

where θ is the Bragg angle, λ is the wavelength of X-rays, β is the full width at half maximum (FWHM).The average crystallite size was found to be in the range of 66-74 nm, which is presented in Table-1. It can be observed that as the concentration of dopant increases the crystallite size decreases, this tendency is due to quantum confinement effects. Further, strain (ε) present in the pure and doped nanophosphors were calculated using Williamson-Hall (W-H) plots [26]

$$\frac{\beta\cos\theta}{\lambda} = \frac{1}{\varepsilon} + \frac{\eta\sin\theta}{\lambda} \quad (2)$$

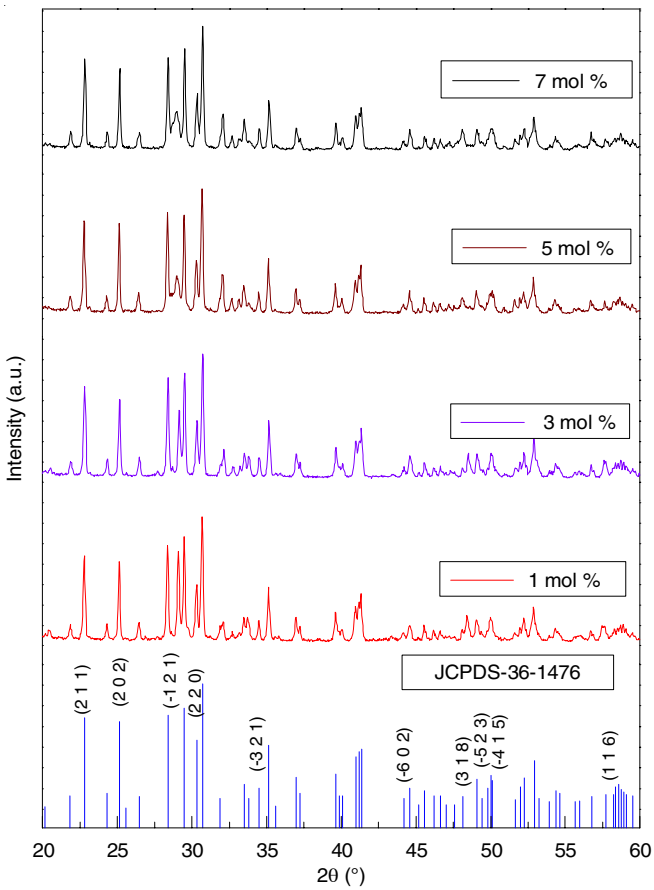

Fig. 1. X-ray diffraction patterns of $Y_2SiO_5:Ce^{3+}$ (undoped, 1, 3, 5 and 7 mol %) nano phosphors

TABLE-1
CRYSTALLITE SIZE AND STRAIN (ε) CALCULATION OF $Y_2SiO_5:Ce^{3+}$ (UNDOPED, 1, 3, 5 AND 7 mol %)

mol %	Crystallite size (nm)		Strain (10^{-4})
	Scherer	W-H	ε
0	30	53	18.00
1	74	84	4.44
3	71	97	10.71
5	70	119	3.49
7	66	89	6.22

where β = FWHM (rad), θ = Bragg′s angle, λ = wavelength of X-rays, η = crystallite size and ε = microstrain. The W-H plots of pure and doped $Y_2SiO_5:Ce^{3+}$ nanophosphors are shown in Fig. 2.The grain size (D) was calculated from the intercept of the straight line and the microstrain was calculated from the slope of curve.

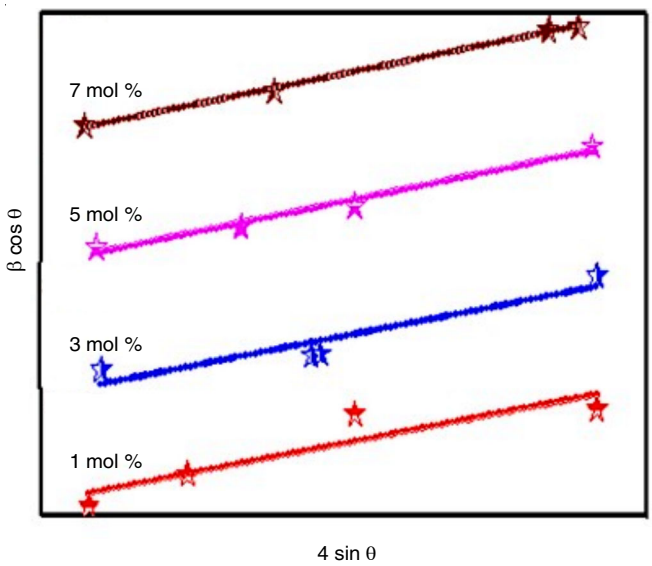

Fig. 2. W-H plots of $Y_2SiO_5:Ce^{3+}$ (1, 3, 5 and 7 mol %)

Surface morphology elemental composition analysis: The surface morphology of the prepared phosphors was analyzed by scanning electron microscopy (SEM). Fig. 3 shows the SEM images recorded for 3 mol % (Fig. 3a and 3b) and 7 mol % (Fig. 3c and 3d) $Y_2SiO_5:Ce^{3+}$ phosphors. It was observed that particles are in spherical shape and agglomerated. This agglomeration of the particles will be attributed to combustion process and subsequent calcination at higher temperature. It was observed that increase in cerium concentration did not influence the morphology of phosphor. The elemental analysis of $Y_2SiO_5:Ce^{3+}$ phosphors were done by the energy dispersive X-ray analysis (EDAX).The profiles of yttrium, silicon, oxygen and cerium were clearly observed in the EDAX spectrum (Fig. 3e), which confirms the incorporation of cerium ions in Y_2SiO_5 host. Inset data shows the elemental composition of cerium, yttrium, silicon and oxygen. The absence of any other peak (impurities) indicates the high purity of sample.

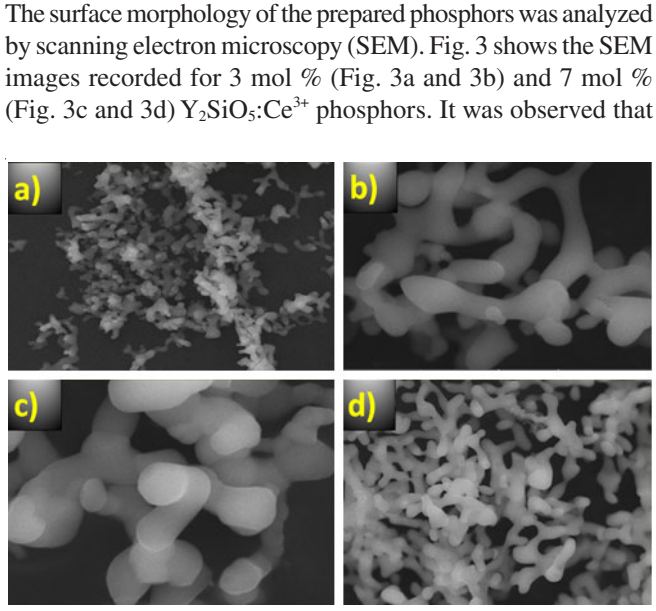

Fig. 3. SEM Micrographs for 3 mol % (a, b) and 5 mol % (c, d) of $Y_2SiO_5:Ce^{3+}$ nanophosphors

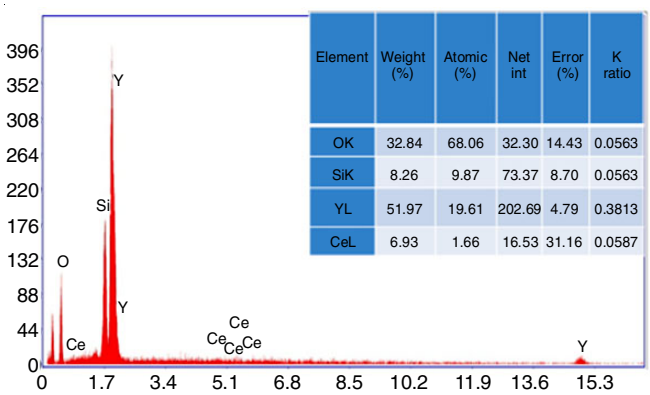

Fig. 3e. EDAX spectrum and elemental composition (Inset) of 3 mol % $Y_2SiO_5:Ce^{3+}$ nanophosphors

FT-IR analysis: To investigate the presence and nature of metal oxygen bonds, FT-IR spectra were recorded for both pure and doped $Y_2SiO_5:Ce^{3+}$ phosphors at room temperature. Fig. 4a-b shows the FT-IR spectra of 3 and 7 mol % cerium doped Y_2SiO_5, respectively. The bands at 510, 447 and 413 cm^{-1} are ascribed to Si-O-Si vibrational bending modes [27], while the band at 552 cm^{-1} is attributed to the presence of Y-O bonds. The weak bands at 714 and 686 cm^{-1} indicate the presence of O-Ce-O bonds vibrations. The bands at 996, 963, 912 and 873 cm^{-1} become more clear and significant on doping of cerium, this also indicates Y_2SiO_5 was well crystallized at 1300 ºC [28].

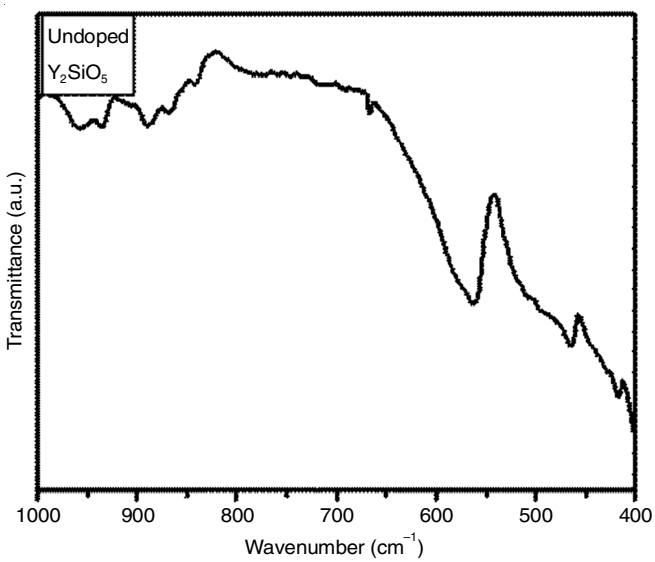

Fig. 4a. Fourier transform infrared spectra of pure$Y_2SiO_5:Ce^{3+}$ phosphors

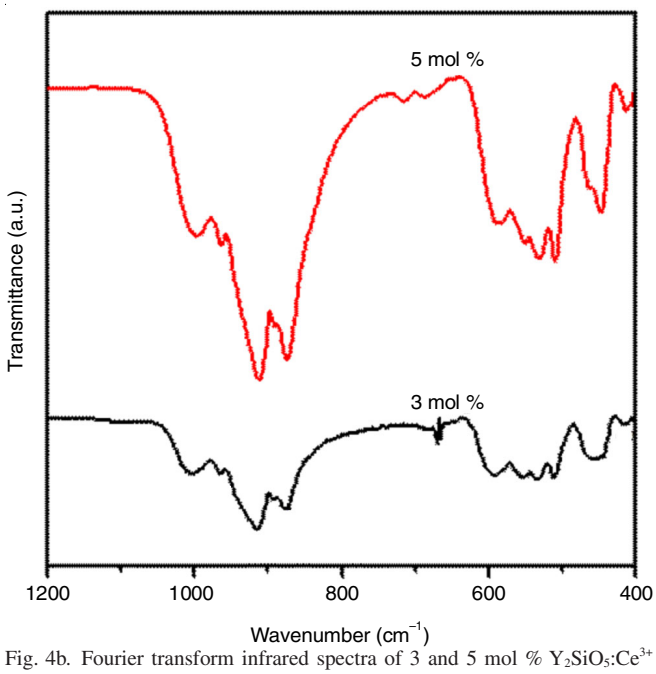

Fig. 4b. Fourier transform infrared spectra of 3 and 5 mol % $Y_2SiO_5:Ce^{3+}$ phosphors

UV-visible absorption studies: The UV-visible spectra of pure and cerium doped Y_2SiO_5 phosphors (1-7 mol %) were recorded (Fig. 5a). The recorded spectra revealed that there exists a strong absorption band around 245 nm. This peak is attributed to charge transfer from valence band to conduction band. The presence of cerium induced few weak absorption bands around 270-310 nm. Fig. 5b shows the Wood-Tauc plots, using which the band gap of pure and doped $Y_2SiO_5:Ce^{3+}$ phosphors were evaluated [29].

$$\alpha h\nu \sim (h\nu - E_g)^n \quad (3)$$

where hν is energy of the photon, α is the optical absorption coefficient and E_g is the band gap respectively. The energy gap was estimated for all the compositions, by plotting $(\alpha h\nu)^n$ *versus* hν in the high absorption range and extrapolating the linear portion of the graph to $(\alpha h\nu)^n = 0$, where n represents

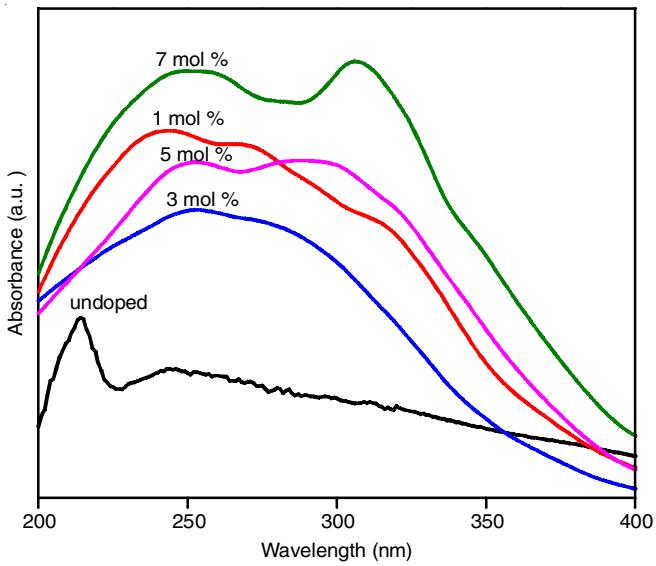

Fig. 5a. UV-visible spectra of undoped and doped $Y_2SiO_5:Ce^{3+}$(1-7 mol %) nano phosphors

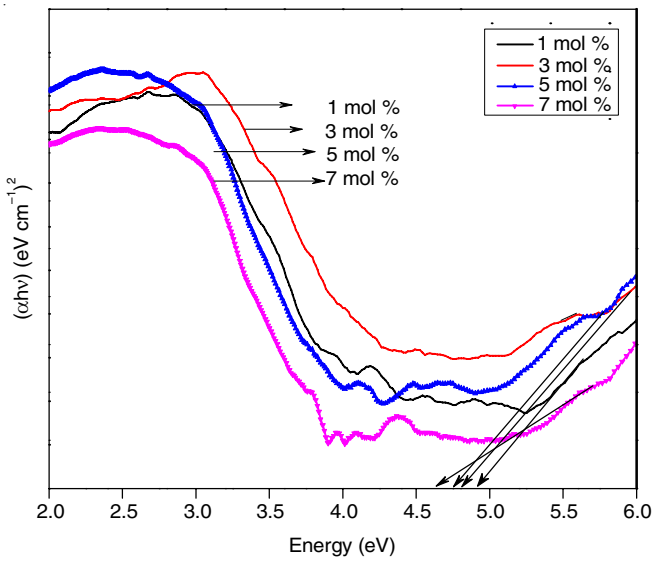

Fig. 5b. Band gap of $Y_2SiO_5:Ce^{3+}$ (1, 3, 5 and 7 mol %) phosphors

the various electronic transitions n = 1/2, 2, 3/2 and 3 for direct allowed, indirect allowed, direct forbidden and indirect forbidden transitions, respectively [30], the band gap calculated for the phosphors were in the range of 4.9 eV – 4.66 eV.

Photoluminescence studies: Excitation spectrum of $Y_2SiO_5:Ce^{3+}$ nanophosphors was recorded for 3 mol % at emission wavelength of 485 nm and is shown in Fig. 6a. The spectra consists of three broad band positioned at 355, 370 and 415 nm. Furthermore, within these absorption bands we have chosen the excitation wavelength of 370 nm to record the emission spectra of the phosphors. Fig. 6b displays the emission spectra of $Y_2SiO_5:Ce^{3+}$ phosphors (1-7mol %) in the range 350- 550 nm. The spectrum consists of two broad peaks at 418 nm, 485 nm and a weak band at 459 nm. The broad peak at 485 nm is ascribed to the electron transition from the 5*d*-lowest energy level of cerium to $^2F_{5/2}$-$^2F_{7/2}$ excited states [31]. That is due to radiative recombination of photogenerated hole with an electron occupying surface defects namely the oxygen vacancies. The F-centers (oxygen ion vacancy occupied by two electrons)/F-

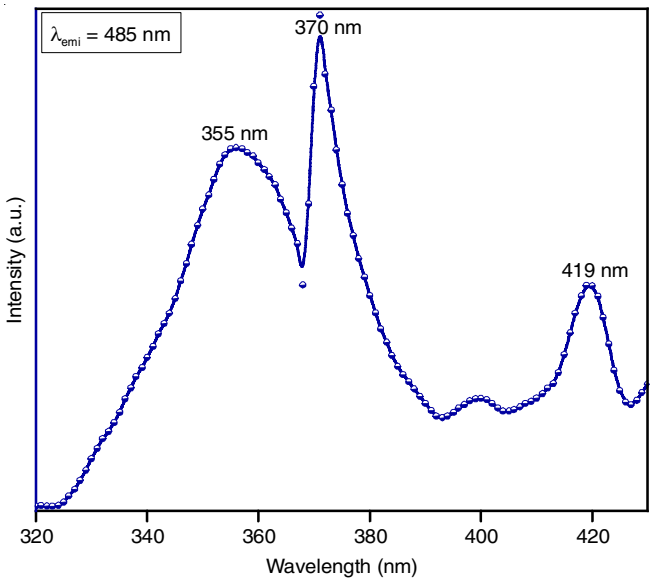

Fig. 6a. Excitation spectra of $Y_2SiO_5:Ce^{3+}$ nanophosphor (λ_{emi} 485 nm)

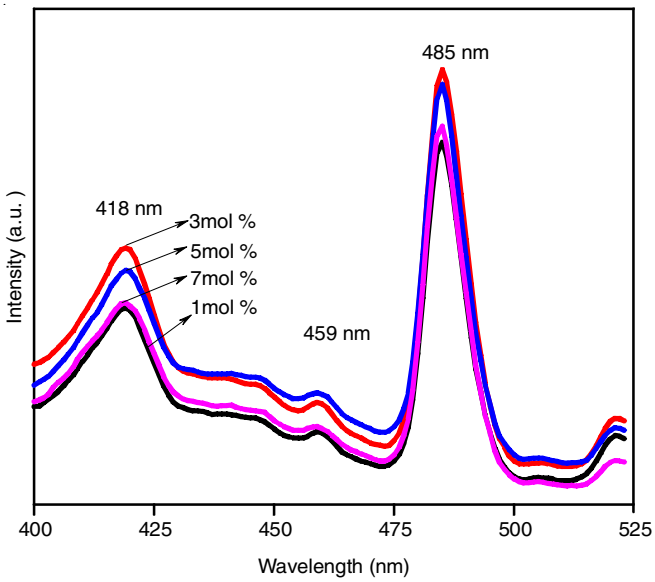

Fig. 6b. Photoluminescence emission spectra of $Y_2SiO_5:Ce^{3+}$ nanophosphor excited at 370 nm

centers (oxygen ion vacancy occupied by single electrons)/ surface states [32-34]. The peaks signify that cerium ions are nanocrystalline capped samples. Due to bandgap shifts, the 5*d* levels are below the conduction band leading to better photoluminescence. In addition to this factor, the surface to volume ratio also contributes for strong photoluminescence intensity [35].

The photoluminescence intensity increases with increase in dopant concentration 1 mol % to 3 mol %. Further increasing the dopant concentration decreased the photoluminescence intensity indicating the concentration quenching. The reason for this quenching can be analyzed by calculating the critical distance (R_c) which can be found by the Blasse formula (eqn. 4) where X_c is the critical concentration, N is the number of cation sites in the unit cell and V is the volume of the unit cell. By substituting the experimental and analytic values N, V and X_c as 4, 1.007×10^{-27} and $0.03R_c$ was found to be 25 Å.

$$R_c = \left(\frac{3V}{4\pi X_c N}\right)^{1/3} \quad (4)$$

In order to determine the type of interaction involved in the energy transfer, Van-Uiter's [36] proposed the following equation:

$$\frac{1}{x} = K\left(1+\beta(X)^{\frac{Q}{3}}\right)^{-1} \quad (5)$$

where I is the integral intensity of emission spectra from 350 to 550 nm, X is the activator concentration, I/X is the emission intensity per activator (X), β and K are the constants for a given host under same excitation condition. As per this equation Q = 3 for the energy transfer among the nearest neighbor ions whereas, if Q = 6, 8 and 10 for dipole-dipole (d-d), dipole-quadrapole (d-q) and quadrapole-quadrapole (q-q) interaction, respectively [37].

Assuming that $\beta(X)^{Q/3} >> 1$ the above equation can be written as:

$$\log\left(\frac{I}{X}\right) = K'\frac{Q}{3}\log(X)\,(K' = \log k - \log\beta) >> 1 \quad (6)$$

Using eqn. 6 multipolar character (Q) is obtained by plotting log (I/X) *versus* log X which is shown in Fig. 6c. The slope and multipolar character was found to be -0.970 and 3, respectively. As Q = 3, it represents that photoluminescence intensity quenching in $Y_2SiO_5:Ce^{3+}$ nanophosphors is due to energy transfer among the nearest neighbours.

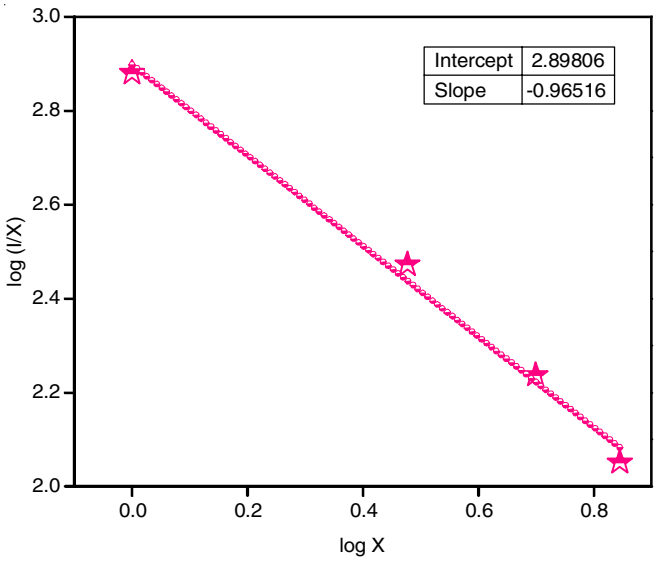

Fig. 6c. Variation of log (I/X) *vs.* log(X) on $Y_2SiO_5:Ce^{3+}$ (1, 3, 5 and 7 mol %)

CIE Chromaticity and correlated colour temperature (CCT) evaluation: One of the main objectives of the work is to find new phosphors for their application in the field of display lamps. In this regard, we studied the colour emission property by CIE coordinates [38] of the $Y_2SiO_5:Ce^{3+}$ (1-7 mol %) phosphors, at an excitation wavelength 370 nm as shown in Fig. 7a. It is observed that colour emission of phosphors lie within the blue region.The set of (x,y) values for various mole concentrations of the phosphors are revealed in the inset table of Fig. 7a. The role of asymmetric ratio and higher energy emission levels leads to the CIE coordinates of blue emission of Ce^{3+} ions.

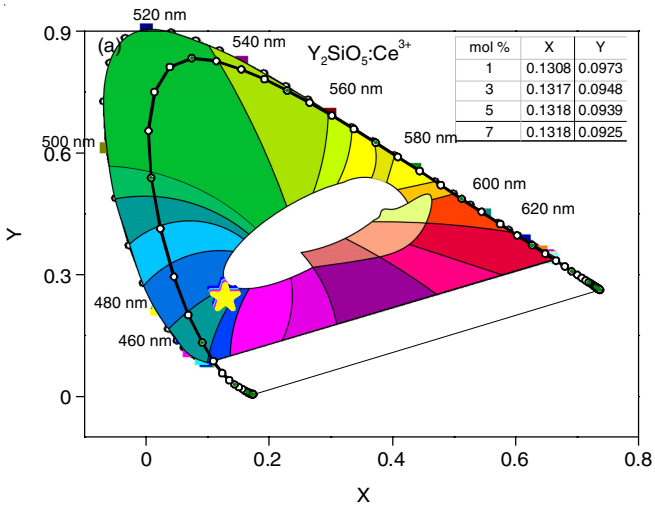

Fig. 7a. CIE diagram of Y_2SiO_5: Ce^{3+} (1-7 mol %) nanophosphor [Inset (x, y) co-ordinate values]

Furthermore correlated colour temperature (CCT) values were calculated from these CIE coordinates, which is shown

in Fig. 7b. If the estimated CCT values are less than 3200 K then the lamp is considered as warm and if it is greater than 4000 K it is considered as cool [39]. In the present work, the CCT value was to be 3268 K, which is slightly above the standard value inferring the cool appearance. Also, the graphical value 3268 K is found to be in good agreement with that calculated using McCamy empirical formula, which was calculated using the relation CCT = -437 n^3 + 3601n^2 - 861n + 5514.31 and found to be 3165 K, where n = (x - x_c)/(y - y_c) and chromaticity epicenter is at x_c = 0.3320 and y_c = 0.1858 [40,41]. All these data conclude that the phosphors are promising materials for their application in LEDs.

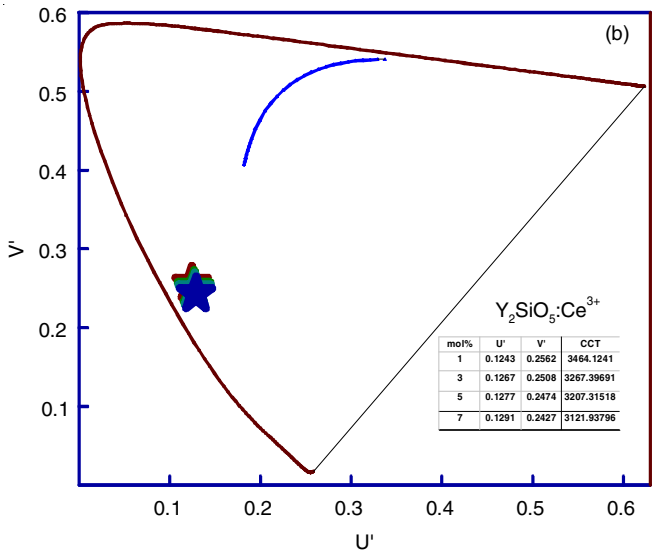

Fig. 7b. Correlated color temperature (CCT) diagram of Y_2SiO_5: Ce^{3+} (1-7 mol %) nanophosphor

Thermoluminescence studies: Fig. 8a shows the variation of thermoluminescence intensity with respect to temperature for $Y_2SiO_5:Ce^{3+}$ (1-7mol %) nanophosphors. There exists a prominent peak at 144 ºC for 1 mol % cerium doped Y_2SiO_5, the maximum thermoluminescence intensity was observed for this concentration, further increasing the concentration of dopant decreased the thermoluminescence intensity. The increase in thermoluminescence intensity for 1 mol % is attributed to surface traps. The decrease in thermoluminescence intensity is due to the ion-ion interaction between the host and dopant, which represents the concentration quenching of dopant [42].

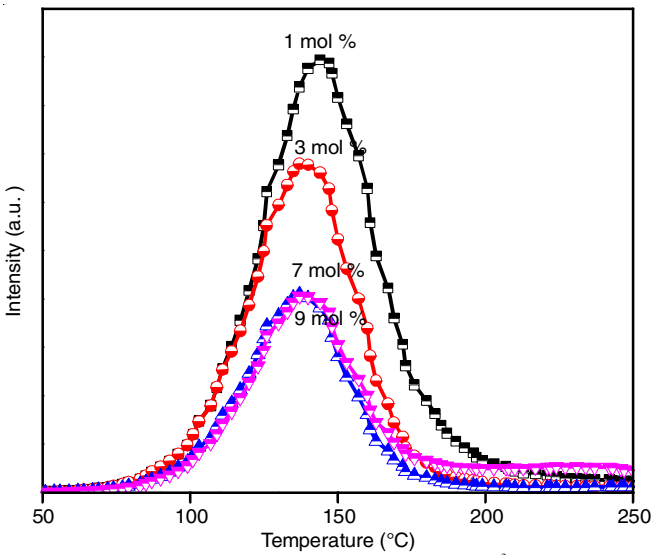

Fig. 8a. Thermoluminescence glow curves of $Y_2SiO_5:Ce^{3+}$ irradiated with 1 KGy γ-dose

Variation of thermoluminescence intensity with γ dose: One of the important properties of a thermoluminescence dosimeter material is that thermoluminescence intensity of these materials follows linearity with respect to absorbed dose and this is the fundamental criteria of a good thermoluminescence dosimeter.The thermoluminescence dose response obeys the following equation:

$$\text{Thermoluminescence (TL)} = a\,(\text{Dose})^b \quad (7)$$

Taking logarithms on both sides of eqn. 7

$$\log(\text{TL}) = \log(a) + b\log(\text{Dose}) \quad (8)$$

where 'a' is a constant and the slope (b = linear factor) can be estimated with linear fit of log (TL) *versus* log (dose). The dose response will be sub-linear; if b < 1 and super linear if b > 1. In the present work, the estimated value of slope b = 0.55 < 1 indicating the dose response is sub-linear with respect to increase in dosage as shown in Fig. 8b.

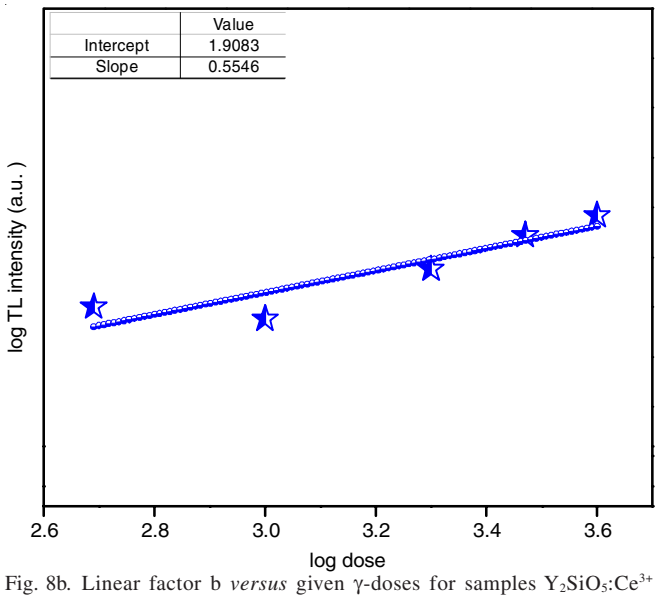

Fig. 8b. Linear factor b *versus* given γ-doses for samples $Y_2SiO_5:Ce^{3+}$ nanophosphor

Fig. 8c shows the thermoluminescence response curve of $Y_2SiO_5:Ce^{3+}$ samples irradiated with different doses of γ-radiation. It is evident from the figure that thermoluminescence intensity glow curve increases linearly with increase in γ dose from 500 Gy to 4 KGy. This increase in thermoluminescence intensity with respect to dose is attributed to creation of large number of traps that are being filled as dose increases. On heating, these traps release their charge carriers resulting different glow peaks. Also from Fig. 8c, it is observed that there exists a shift in the maximum temperature (T_m) from 500 Gy to 1 KGy dose. This shift in the T_m is perceived as a result of second order kinetics. The variation of intensity *versus* dose gives a simple method to discriminate first or second order kinetics.

Evaluation of kinetic parameters: The dosimetry properties of thermoluminescence materials mainly depend on the

TABLE-2
KINETIC PARAMETERS OF $Y_2SiO_5:Ce^{3+}$ (1 mol %) NANOPHOSPHORS WITH DIFFERENT γ DOSES

Dose (kGy)	T_1	T_2	T_m (°C)	ω	b (μ_g)	E_{avg}	Frequency factor (s^{-1})
0.5	393	439	416	46.43	1.8 (0.50)	1.01	5.52×10^{11}
1.0	389	432	411	43.68	1.7 (0.59)	1.02	1.08×10^{12}
2.0	389	432	411	42.87	1.5 (0.476)	0.99	4.51×10^{11}
3.0	389	431	410	42.47	1.8 (0.501)	0.5	8.94×10^{12}
4.0	390	432	411	42.18	1.8 (0.500)	1.09	8.27×10^{12}

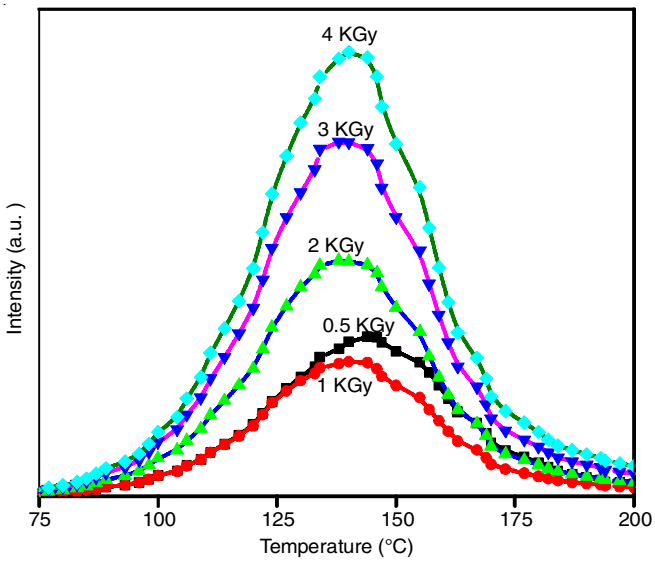

Fig. 8c. Effect of γ-dose on thermoluminescence glow curves of $Y_2SiO_5:Ce^{3+}$ nanophosphor (heating rate of 3 °C s^{-1})

kinetic parameters. They give useful information about emission behaviour of the phosphor. These parameters are estimated by using Chen's peak shape method [43-46].

In this method, the shape of glow curves provides the order of kinetics. If the shape is symmetrical then, it is second order or if it possess asymmetrical shape then it is first order in nature. Based on the shape of glow curve, parameters like trap depth, frequency factor can be determined. The following equations are employed to estimate the kinetic parameters.

$$E_\alpha = C_\alpha\left(\frac{KT^2m}{\propto}\right) - b_\alpha(2kT_m) \qquad (9)$$

where $\alpha = \tau$, δ and ω with $\tau = T_m - T_1$, $\delta = T_2 - T_m$ and $\omega = T_2 - T_1$

$C_\tau = 1.51 + 3.0(\mu_g - 0.42)$, $b_\tau = 1.58 + 4.2(\mu_g - 0.42)$

$C_\delta = 0.976 + 7.3(\mu_g - 0.42)$, $b_\delta = 0$

$C_\omega = 2.52 + 10.2(\mu_g - 0.42)$, $b_\omega = 1$

$$\frac{\beta E}{kT_{m^2}} = s\exp\left\{\frac{-E}{kT_{m^2}}\right\}[1+(b-1)\Delta_m]$$

where $\Delta = 2kT/E$; $\Delta_m = 2kT_m/E$ and β is the linear heating rate; K is the Boltzmann constant (8.6×10^{-5} eV); S is the frequency factor and (b) is the order of kinetics.

From Table-2, we can analyze that the value of μ_g which is ranging from 0.47 to 0.59 and it follows second order kinetics, the activation energy lies between 0.5 eV - 1.09 eV and the frequency factor is of the order of 10^{11}-10^{12} S^{-1}.

Conclusion

$Y_2SiO_5:Ce^{3+}$ phosphors were successfully prepared by combustion method. The XRD data indicates monoclinic structure of the prepared phosphors with crystallite size ranging between 66-74 nm. The UV-visible absorption studies indicate the presence of weak absorption bands in the range 270-310 nm, which corresponds to metal oxygen bonds. The optical band gap was calculated using Wood-Tauc relation and it is found to be between 4.9 eV - 4.66 eV. The surface morphology was analyzed by SEM and shows the porous structure. The photoluminescence peaks observed at 428, 459 and 485 nm are assigned to the electronic transitions 5*d*-4*f* when excited at 370 nm. The photoluminescence spectrum shows a broad emission peak centered at 485 nm (blue emission). Hence, this phosphor can be used as host for blue light emission in display devices. Further, the phosphor has CIE chromaticity coordinates at (X, Y) and CCT value of 3268 K, which implies that the material can be used in warm light display applications. The effect of concentration of cerium dopant on the thermoluminescence intensity of Y_2SiO_5 phosphor has been discussed. The concentration quenching was observed at 1 mol % cerium doping. An investigation of effect of γ dose was made and the kinetic parameters indicate that $Y_2SiO_5:Ce^{3+}$ is a competent material in the dosimetric applications.The kinetic parameters were estimated using the Chen's peak relations and found to be second order with activation energy 0.5 eV - 1.09 eV.

CONFLICT OF INTEREST

The authors declare that there is no conflict of interests regarding the publication of this article.

REFERENCES

1. C.R. Ronda, *J. Lumin.*, **72-74**, 49 (1997); https://doi.org/10.1016/S0022-2313(96)00374-2.
2. Y. Ren, G. Brown, A. Ródenas, S. Beecher, F. Chen and A.K. Kar, *Opt. Lett.*, **37**, 3339 (2012); https://doi.org/10.1364/OL.37.003339.
3. L.H. Slooff, A. Van Blaaderen, A. Polman, G.A. Hebbink, S.I. Klink, F.C.J.M. Van Veggel, D.N. Reinhoudt and J.W. Hofstraat, *J. Appl. Phys.*, **91**, 3955 (2002); https://doi.org/10.1063/1.1454190.
4. D. Weller and W. Reim, *Appl. Phys., A Solids Surf.*, **49**, 599 (1989); https://doi.org/10.1007/BF00616985.
5. S. Liang, M. Shang, H. Lian, K. Li, Y. Zhang and J. Lin, *J. Mater. Chem. C Mater. Opt. Electron. Devices*, **5**, 2927 (2017); https://doi.org/10.1039/C6TC05499D.
6. T. Grzyb, A. Szczeszak, J. Rozowska, J. Legendziewicz and S. Lis, *J. Phys. Chem. C*, **116**, 3219 (2012); https://doi.org/10.1021/jp208015z.
7. Z. Sun, M. Li and Y. Zhou, *J. Eur. Ceram. Soc.*, **29**, 551 (2009); https://doi.org/10.1016/j.jeurceramsoc.2008.07.026.

8. X. Qin, Y. Ju, S. Bernhard and N. Yao, *Mater. Res. Bull.*, **42**, 1440 (2007); https://doi.org/10.1016/j.materresbull.2006.11.021.
9. X. Ouyang, A.H. Kitai and R. Siegele, *Thin Solid Films*, **254**, 268 (1995); https://doi.org/10.1016/0040-6090(94)06255-J.
10. M. Mitsunaga, R. Yano and N. Uesugi, *Opt. Lett.*, **16**, 1890 (1991); https://doi.org/10.1364/OL.16.001890.
11. Y. Liu, C.-N. Xu, H. Matsui, T. Imamura and Tadahiko Watanabe, *J. Lumin.*, **87-89**, 1297 (2000); https://doi.org/10.1016/S0022-2313(99)00597-9.
12. X. Ouyang, A.H. Kitai and T. Xiao, *J. Appl. Phys.*, **79**, 3229 (1996); https://doi.org/10.1063/1.361269.
13. W. Ya-qin, H. Jian-Feng, C. Zheng-hui and C. Li-yun, *J. Compos. Mater.*, **46**, 409 (2012); https://doi.org/10.1177/0021998311425618.
14. T. Karner, V.V. Laguta, M. Nikl, T. Shalapska and S. Zazubovich, *J. Phys. D Appl. Phys.*, **47**, 065303 (2014); https://doi.org/10.1088/0022-3727/47/6/065303.
15. S. Saha, P.S. Chowdhury and A. Patra, *J. Phys. Chem. B*, **109**, 2699 (2005); https://doi.org/10.1021/jp0462106.
16. L. Guerbous and A. Boukerika, *J. Nanomater.*, **2015**, Article ID 617130 (2015); https://doi.org/10.1155/2015/617130.
17. L. Parashuram, S. Sreenivasa, S. Akshatha, V.U. Kumar and S. Kumar, *Asian J. Org. Chem.*, **6**, 1755 (2017); https://doi.org/10.1002/ajoc.201700467.
18. Y. Lin, S. Inoue, Y. Matsumura and J.C. Chen, *AIP Adv.*, **7**, 015208 (2017); https://doi.org/10.1063/1.4975151.
19. G. Wang, L. Gao, H. Zhu and W. Zhou, *Front. Mater. Sci.*, **10**, 197 (2016); https://doi.org/10.1007/s11706-016-0340-1.
20. A. Nohara, S. Takeshita, Y. Iso and T. Isobe, *J. Mater. Sci.*, **51**, 3311 (2016); https://doi.org/10.1007/s10853-015-9645-1.
21. Y. Zhu, G. Xu, T. Guo, H. Hou and S. Tan, *J. Alloys Compd.*, **720**, 105 (2017); https://doi.org/10.1016/j.jallcom.2017.05.252.
22. K. Dhanalakshmi, A. Jagannatha Reddy, D.L. Monika, R. Hari Krishna and L. Parashuram, *J. Non-Cryst. Solids*, **471**, 195 (2017); https://doi.org/10.1016/j.jnoncrysol.2017.05.040.
23. K.C. Patil, S.T. Aruna and T. Mimani, *Curr. Opin. Solid State Mater. Sci.*, **6**, 507 (2002); https://doi.org/10.1016/S1359-0286(02)00123-7.
24. A.S. Mukasyan, P. Epstein and P. Dinka, *Proc. Combust. Inst.*, **31,** 1789 (2007); https://doi.org/10.1016/J.PROCI.2006.07.052.
25. J. Kaur, Y. Parganiha, V. Dubey, D. Singh and D. Chandrakar, *Superlattices Microstruct.*, **73**, 38 (2014); https://doi.org/10.1016/j.spmi.2014.05.009.
26. G.K. Williamson and W.H. Hall, *Acta Metall.*, **1**, 22 (1953); https://doi.org/10.1016/0001-6160(53)90006-6.
27. V. Dubey, R. Tiwari, R. Shrivastava, C. Markande, O. Verma, J.K. Saluja, Y. Parganiha and K.V.R. Murthy, *J. Disp. Technol.*, **12**, 171 (2016); https://doi.org/10.1109/JDT.2015.2488359.
28. L. Muresan, M. Stefan, E. Bica, M. Morar, E. Indrea and E.J. Popovici, *J. Optoelectron. Adv. Mater.*, **2**, 131 (2010).
29. J. Tauc and A. Menth, *J. Non-Cryst. Solids*, **8-10**, 569 (1972); https://doi.org/10.1016/0022-3093(72)90194-9.
30. R. Naik, S.C. Prashantha, H. Nagabhushana, H.P. Nagaswarupa, D.M. Jnaneshwara, P.B. Devaraja and G.P. Darshan, *AIP Conf. Proc.*, **1832**, 050035 (2017); https://doi.org/10.1063/1.4980268.
31. L.E. Muresan, A.I. Cadis, I. Perhaita, B.F. Oprea and D.T. Silipas, *AIP Conf. Proc.*, **1565**, 193 (2013); https://doi.org/10.1063/1.4833726.
32. Y. Parganiha, J. Kaur, V. Dubey and K.V.R. Murthy, *Mater. Sci. Semicond. Process.*, **31**, 715 (2015); https://doi.org/10.1016/j.mssp.2014.12.070.
33. V. Dubey, S. Agrawal and J. Kaur, *Optik*, **126**, 1 (2015); https://doi.org/10.1016/j.ijleo.2014.06.175.
34. V. Dubey, J. Kaur and S. Agrawal, *Mater. Sci. Semicond. Process.*, **31**, 27 (2015); https://doi.org/10.1016/j.mssp.2014.10.052.
35. N. Karar and H. Chander, *J. Phys. D Appl. Phys.*, **38**, 3580 (2005); https://doi.org/10.1088/0022-3727/38/19/006.
36. L.G. Van Uitert, *J. Electrochem. Soc.*, **114**, 1048 (1967); https://doi.org/10.1149/1.2424184.
37. H. Wu, Y. Wang, Y. Hu, L. Deng and W. Xie, *J. Phys. D Appl. Phys.*, **42**, 125406 (2009); https://doi.org/10.1088/0022-3727/42/12/125406.
38. R. Naik, S.C. Prashantha, H. Nagabhushana, H.P. Nagaswarupa, K.S. Anantharaju, S.C. Sharma, B.M. Nagabhushana, H.B. Premkumar and K.M. Girish, *J. Alloys Compd.*, **617**, 69 (2014); https://doi.org/10.1016/j.jallcom.2014.07.100.
39. D.B. Judd, *J. Opt. Soc. Am.*, **26**, 421 (1936); https://doi.org/10.1364/JOSA.26.000421.
40. J. Schanda and M. Danyi, *Color Res. Appl.*, **2**, 161 (1977); https://doi.org/10.1002/col.5080020403.
41. G.A. Kumar, M. Pokhrel, A. Martinez, R.C. Dennis, I.L. Villegas and D.K. Sardar, *J. Alloys Compd.*, **513**, 559 (2012); https://doi.org/10.1016/j.jallcom.2011.11.006.
42. G. Sharm, P. Chawla, S.P. Lochab and N. Singh, *Chalcogenide Lett.*, **6**, 445 (2009).
43. R. Chen and J. Appl. Phys, *J. Phys. D*, **2**, 371 (1969); https://doi.org/10.1088/0022-3727/2/3/309.
44. M. Gokce, K.F. Oguz, T. Karali and M. Prokic, *J. Phys. D Appl. Phys.*, **42**, 105412 (2009); https://doi.org/10.1088/0022-3727/42/10/105412.
45. Y. Wang and L. Wang, *J. Appl. Phys.*, **101**, 053108 (2007); https://doi.org/10.1063/1.2435822.
46. Z.-X. Yuan, C. Chang, D. Mao and W. Ying, *J. Alloys Compd.*, **377**, 268 (2004); https://doi.org/10.1016/j.jallcom.2004.01.063.